Available online at www.sciencedirect.com
SCIENCE DIRECT®
Journal of Power Sources 145 (2005) 546–554
JOURNAL OF POWER SOURCES
www.elsevier.com/locate/jpowsour

Numerical prediction of concentration and current distributions in PEMFC

Fang-Bor Weng*, Ay Su, Guo-Bin Jung, Yen-Chiao Chiu, Shih-Hung Chan

Department of Mechanical Engineering & Fuel Cells Research Center, Yuan Ze University, 135 Yuan-Tung Rd., Chung-Li, Tao Yuan, 320 Taiwan, ROC

Accepted 11 January 2005
Available online 18 July 2005

Abstract

In this study, we present a rigorous 3-D mathematical model, to treat prediction and analysis of proton exchange membrane fuel cells (PEMFC) species concentration and current density distributions in different flow field patterns and operating conditions. The model is based on the solution of the conservation equations of mass, momentum, species and electric current in a fully integrated finite-volume solver using the CFDRC commercial code. The polarization curve of serpentine flow pattern is well correlated with experimental data. The cell performance with parallel straight, serpentine and interdigitated flow patterns are calculated and compared. The simulation results reveal that serpentine and interdigitated flow patterns show strong convection and high mass transfer. However, they also have larger pressure loss. In addition, the effects of operating temperature and relative humidity are also studied. Non-uniform distributions of concentration and current density appear at high temperature, high current density and low humidity operation, which could lead to an unstable cell performance.

Keywords: Fuel cell; Numerical modeling; Flow pattern; Polarization curve

1. Introduction

Fuel cell, which transforms the chemical energy into electricity at high efficiency, high power density, is considered to be a promising power source, especially for transportation application. Its performance and efficiency must be improved, and the issues of cost, reliability and safety need to be considered to realize the fuel cell commerciality. In order to enhance its performance and reliability, it is necessary to learn more about the mechanism that causes the performance loss, such as, non-uniform concentration, current density distributions, high ionic resistance due to dry membrane, or high diffusive resistance due to the flooding on the cathode. The flow field and water/thermal management of fuel cell need optimal design to achieve high performance and reliability. The numerical modeling and dedicated experimental technique development will be the effective tools to improve the optimal design of fuel cell system.

To understand the mechanism of fluid mechanics and electrochemical processes within a fuel cell, the first two models were published in the early 1990s by Springer et al. [1] and Bernardi and Verbrugge [2]. These models are one-dimensional and only account for simple diffusive mass transport and electrochemical kinetics. After that, several two-dimensional models have been presented by researchers [3–5]. Most of these models compute the flow field along a single channel to study the reaction species and current density distributions. Results of polarization curve are well correlated with experimental data. Um et al. [6] considered the two-phase flow model within porous diffusion layer and flow channel to study the flooding of GDL and gas channel, which impedes gas flow and also reduces efficiency.

Recently, three-dimensional models based on die computational fluid dynamics approach were presented and computed by commercial software [7,8] or self-developed

* Corresponding author. Tel.: +886 3 463 8800x859; fax: +886 3 455 5574.
E-mail address: fangbor@saturn.yzu.edu.tw (F.-B. Weng).

0378-7753/$ – see front matter © 2005 Elsevier B.V. All rights reserved.
doi:10.1016/j.jpowsour.2005.01.078

Nomenclature

F	Faraday constant
i_F	in porous media, the current flowing through the solid parts of the porous matrix (A)
i_S	in porous media, the current flowing through the pores (A)
j_0	reference current (A m^{-3})
J_i	diffusion flux
U	velocity (m s^{-1})
Y_i	mass-fractions of ith species

Greek letters

α_a	anode kinetic constant
α_c	cathode kinetic constant
ε	porosity
κ	permeability (m^2)
$[\Lambda]$	the near-wall molar concentration of the reacting species
μ	viscosity (m^2 s^{-1})
ω_i	production rates of ith species in the gas phase
ρ	pressure (N m^{-2})
Φ_S	solid potential (V)
Φ_F	fluid potential (V)
τ	shear force tension

numerical model of the SIMPLE algorithm [9–11]. The three-dimensional models account for the effect of the complex geometry, specifically interdigitated flow field. They allow a parametric study for a realistic flow field, concentration and current distributions. The simulation results are well compared with the experimental data of polarization curve. However, the influence of flow field design upon concentration and current density distributions is less discussed.

Mench et al. [12] proved that the effects of cathode stoichiometry variation and transient flooding on local current density affect the current distribution. When voltages are 0.9–0.6 V (electrochemical reaction controlled region), the current density in downstream is higher than upstream. On the other hand, when the voltages are 0.4–0.2 V, the current density in upstream is higher than downstream. There are significant progresses on developed experimental technique for the measurement of current, species, temperature distributions [13] and flow field flooding (water content) [14]. The efforts on fuel cell modeling and experimental measurement technique are valuable for fuel cell developers, which can optimize fuel cell designs and operations.

The major objectives of this work are to: (1) modify a 3-D PEM fuel cell model to predict the cell performance, concentration and current density distributions without counting the thermal and two-phase flow effect, (2) study the effect of the flow field patterns on concentration and current density distributions, which can aid in the design of the flow field plates and (3) study the cell temperature and relative humidity effects on the uniformity of species concentration and current density.

2. Model development

The PEMFC structure includes the flow field plate, gas diffusion, catalyst layer, membranes and bipolar plate, etc. (see Fig. 1). Parallel straight, serpentine flow and interdigitated flow patterns are shown in Fig. 2. Tables 1 and 2 are the dimensions and properties of the flow field plate, membrane, electrode material properties and the initial operating conditions used in the numerical simulation.

The numerical calculations are based on solution of the conservation equations of mass, momentum, energy, current and species transport on a computational grid using finite-volume, finite-difference methodologies. The key elements to modeling fuel cells are the transport phenomena through porous media, heterogeneous reactions

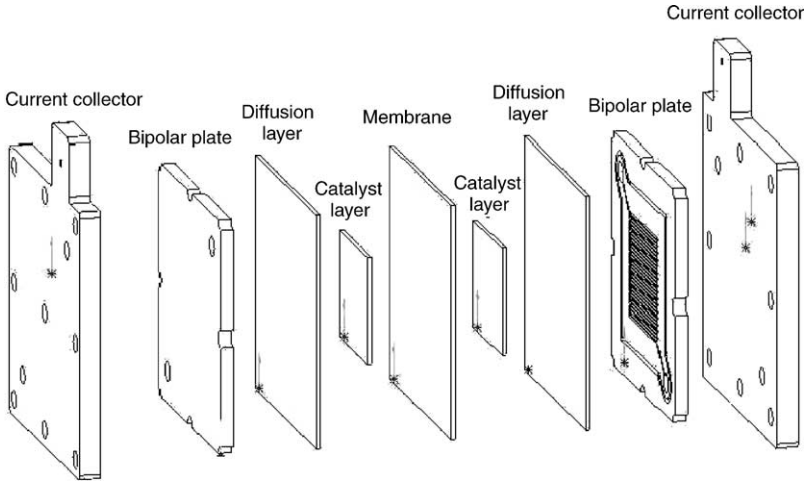

Fig. 1. Schematic illustration of PEMFC.

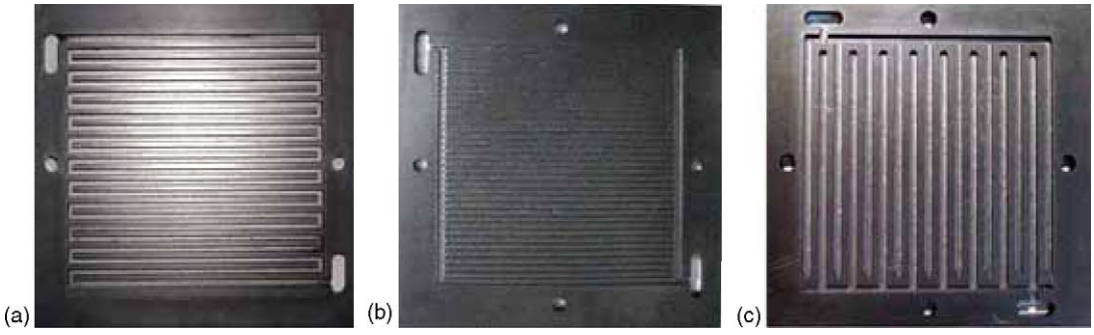

Fig. 2. (a) Parallel straight flow pattern, (b) serpentine flow pattern and (c) interdigitated flow pattern.

Table 1
Dimensions, properties and parameters for the numerical model

Channel length (mm)	50
Channel width (mm)	1.2
Channel depth (mm)	1
Rib width (mm)	1.2
Diffusion layer thickness (mm)	0.2
Catalyst layer thickness (mm)	Anode: 0.018; cathode: 0.026
Membrane thickness (mm)	0.035
Total reaction area (cm^2)	25
Effective diffusivity	Bruggeman model, $\tau = 7$ for membrane Bruggeman model, $\tau = 1.5$ for diffusion and catalyst layer
Membrane permeability (m^2)	1.8×10^{-18}
Diffusion and catalyst layer permeability (m^2)	1.76×10^{-11}
Membrane porosity	0.28
Diffusion and catalyst layer porosity	0.4
Air and fuel side pressure (atm)	1
Transfer coefficient (Tafel constants) at anode	0.5
Concentration dependence at anode	0.5(H_2)
Reference current density at anode ($(A\,m^{-3})(m^3\,(kg\,mol\,H_2)^{-1})^{1/2}$)	9.23×10^8
Transfer coefficients (Tafel constants) at cathode	1.5
Concentration dependence at cathode	1.0(O_2)
Reference current density at cathode ($((A\,m^{-3})(m^3\,(kg\,mol\,H_2)^{-1}))^{1/2}$)	1.05×10^6
Diffusion and catalyst layer conductivity ($l\,(\Omega\,m)^{-1}$)	100

within porous electrodes and the coupling between mass transports, electrochemical reactions and current–potential fields.

Table 2
Operating conditions for the numerical model

H_2 at fuel inlet ($cm^3\,min^{-1}$)	300
Anode gas	Humidified hydrogen (0, 50, 100%RH)
O_2 at fuel inlet ($cm^3\,min^{-1}$)	300
Cathode gas	Humidified oxygen (0, 50, 100%RH)
Operating pressure (atm)	1
Operating temperature (°C)	30, 50, 70

The main assumptions of the modeling are:

1. steady state;
2. laminar flow;
3. isothermal;
4. all gases are treated as ideal gas;
5. gas phase flow in catalyst layer, gas diffusion layer and channel flow field, without the effects of vaporization and condensation;
6. the Stefan–Maxwell equations for multi-species diffusion;
7. Butler–Volmer equation is used to describe electrochemical reactions within the catalyst layers;
8. Nerst–Planck equation is used for the transport of protons through the membrane;
9. Ohm's law is applied across whole region of the polarization curve;
10. gravity effect is neglected.

2.1. Channel flow field

According to assumptions, these conservation equations of mass, momentum and species in flow channel are follows:

Mass conservation:

$$\frac{\partial \rho}{\partial t} + \nabla(\rho \vec{U}) = 0 \tag{1}$$

Momentum conservation:

$$\begin{aligned} X\text{-axis}: &\quad \frac{\partial \rho u}{\partial t} + \nabla \cdot (\rho \vec{U} u) = -\frac{\partial p}{\partial x} + \nabla(\mu\, \nabla u) \\ Y\text{-axis}: &\quad \frac{\partial \rho v}{\partial t} + \nabla \cdot (\rho \vec{U} v) = -\frac{\partial p}{\partial y} + \nabla(\mu\, \nabla v) \\ Z\text{-axis}: &\quad \frac{\partial \rho w}{\partial t} + \nabla \cdot (\rho \vec{U} w) = -\frac{\partial p}{\partial z} + \nabla(\mu\, \nabla w) \end{aligned} \tag{2}$$

where ρ is the fluid density, p the pressure and μ is the dynamic viscosity.

Species conservation:

$$\frac{\partial}{\partial t}(\varepsilon \rho Y_i) + \nabla \cdot (\varepsilon \rho \vec{U} Y_i) = \nabla J_i \tag{3}$$

where Y_i is the mass-fraction of ith species and J_i is the diffusive flux.

The species diffusion flux may be written as:

$$J_i = \rho D_i \nabla Y_i + \frac{\rho Y_i}{M} D_i \nabla M - \rho Y_i \sum_j D_j \nabla Y_j - \rho Y_i \frac{\Delta M}{M} \sum_j D_j Y_j \quad (4)$$

where M is the mixture molecular weight and D_i is the effective mass diffusion coefficient of species i.

$$D_i = D_{i,\mathrm{FS}} \varepsilon^{\tau} \quad (5)$$

where $D_{i,\mathrm{FS}}$ is the free stream diffusion coefficient of the ith species, ε porosity of the medium and τ is the tortuosity of the medium. It is a common practice to use tortuosity value of 1.5 in Eq. (5), resulting in the so-called Bruggeman model, and the same value was adopted in our simulations due to lack of better information.

2.2. Gas diffusion layer

The main assumption is isotropic porous media, their mass and momentum equations are effected by porosity ε and permeability κ.

These equations are showed as:

Mass conservation:

$$\frac{\partial}{\partial t}(\varepsilon\rho) + \nabla \cdot (\varepsilon\rho\vec{U}) = 0 \quad (6)$$

where ρ is the fluid density.

Momentum conservation:

$$\frac{\partial}{\partial t}(\varepsilon\rho) + \nabla \cdot (\varepsilon\rho\vec{U} \cdot \vec{U}) = -\varepsilon\nabla\rho + \nabla \cdot (\varepsilon\tau) + \varepsilon B + \frac{\varepsilon^2 \mu \vec{U}}{k} \quad (7)$$

where ρ is the fluid density, p the pressure, μ the dynamic viscosity, τ shear force tensor, $\vec{U}$ the flow velocity vector, ε porosity of the medium, B the body force vector and κ is a quantity representing the square of the effective volume to surface area ratio of the porous matrix.

The last term in Eq. (7) represents Darcy's drag force imposed by pore walls on the fluid within the pores, and usually results in a significant pressure drop across the porous medium. Species conservation equation in the gas diffusion layer is the same as in flow field. The continuity of current within any material under electroneutral conditions leads to:

$$\nabla \cdot i = 0 \quad (8)$$

where i is the current density vector.

2.3. Catalyst layer

The mass and momentum equation in the catalyst layer is the same in the gas diffusion layer. The mass conservation equations for individual gas phase species (i.e., for $i = 1, \ldots, N_{\mathrm{G}}$) may be written as:

$$\frac{\partial}{\partial t}(\varepsilon\rho Y_i) + \nabla \cdot (\varepsilon\rho\vec{U}Y_i) = \nabla J_i + \dot{\omega}_i \quad (9)$$

where Y_i are the mass fractions of the ith species and $\dot{\omega}_i$ are the production rates of the ith species in the gas phase. $\dot{\omega}_i$ due to heterogeneous electrochemical reactions within porous media.

The species diffusion flux may be written as:

$$J_i = \rho D_i \nabla Y_i + \frac{\rho Y_i}{M} D_i \nabla M - \rho Y_i \sum_j D_j \nabla Y_j - \rho Y_i \frac{\Delta M}{M} \sum_j D_j Y_j \quad (10)$$

where the M is the mixture molecular weight. The first term represents Fickian diffusion due to concentration gradients. The last three terms are correction terms necessary to satisfy the Stefan–Maxwell equations for multicomponent species i within the porous medium, and depend on the porosity, ε, and tortuosity, τ, of the medium:

$$D_i = D_{i,\mathrm{FS}} \varepsilon^{\tau} \quad (11)$$

where D_i is the free stream diffusion coefficient of the ith species.

In the case of electrochemical reaction, the volumetric production rate of a given species is expressed by the ratio of the transfer current, j_{T}, and the Faraday constant, F:

$$\omega_i = (a_i'' - a_i') \frac{j_{\mathrm{T}}}{F} \quad (12)$$

where a_i'' and a_i' are the stoichiometric coefficients of the products and reactants, respectively. The transfer current, j_{T}, is obtained from the Butler–Volmer condition, and may be written in its most general form as:

$$j_{\mathrm{T},j} = \frac{j_{0,j}}{\prod_{k=1}^{N} [\Lambda_{k,\mathrm{ref}}]^{\alpha_{k,j}}} \left[\exp\left(\frac{\alpha_{\mathrm{a},j} F}{RT} \eta \right) - \exp\left(\frac{\alpha_{\mathrm{c},j} F}{RT} \eta \right) \right] \times \prod_{k=1}^{N} [\Lambda_k]^{\alpha_{k,j}} \quad (13)$$

where j_0 is the reference current at a known open circuit voltage and $\alpha_{\mathrm{a},j}$ and $\alpha_{\mathrm{c},j}$ are kinetic constants. $[\Lambda]$ represents the near-wall molar concentration of the reacting species, N the total number of reacting species and $\alpha_{k,j}$ are the concentration exponents. Species conservation equation in the gas diffusion layer is the same in flow field. The continuity of current within any material under electroneutral conditions leads to:

$$\nabla \cdot i = 0 \quad (14)$$

where i is the current density vector. When the material is a porous electrode, the current may split into two parts: one flowing through the polymer electrolyte (ionic phase) and the other flowing through the solid parts or electronic phase of

the porous matrix. If these components are denoted by i_F and i_S, respectively, Eq. (14) can be rewritten as:

$$\nabla i_F + \nabla i_S = 0 \tag{15}$$

During electrochemical reactions within a porous solid, flow of current results from charge transfer between the ionic and electronic phase. This results in a source in one of the phases and a sink in the other phase. Thus, Eq. (15) may be written as:

$$-\nabla \cdot i_F + \nabla \cdot i_S = j_T \left[\frac{S}{V}\right]_{eff} = \left[\frac{S}{V}\right]_{eff} \sum_{j=1}^{N_{steps}} j_{T,j} \tag{16}$$

$[S/V]_{eff}$ is the effective surface-to-volume ratio.

Application of Ohm's law to Eq. (15), yields:

$$\nabla \cdot (\sigma_F \nabla \Phi_F) = -\nabla \cdot (\sigma_S \nabla \Phi_S) = j_T \left[\frac{S}{V}\right]_{eff} \tag{17}$$

where Φ_F and Φ_S are the electric potentials of the ionic and electronic phases, respectively.

2.4. Proton exchange membrane

In the proton exchange membrane, governing equations are the same as in the catalyst layer, but without any chemical reaction. The membrane proton conductivity is correlated by the experimental data, Springer et al. [1], which are dependent on temperature and water content.

The solution to the above set of conservation equations is performed using a finite-volume scheme on arbitrary unstructured mesh topology within the framework of the commercial CFD code CFD-ACE+, provided by CFDRC software.

2.5. Computational domain

We describe a detailed three-dimensional model of transport phenomena and performance within the PEMFC including gas channel, gas diffusion layer, catalyst layer and membrane. The dimensions of the computational domains have 27 elements in the *x*-direction, 84 elements in the *y*-direction, 42 elements in the *z*-direction, for a total of about 95,256 elements and 198,660 nodes. The gird distributions and cross-section of concentration and current density are shown in Su et al. [8]. The species concentrations are calculated at the interface of catalyst/GDL, while the current density distributions are at the current collect plate.

2.6. Experimental details

An experimental system is setup to obtain the current/voltage polarization curves. Graphite plate is used as a current collector with serpentine flow pattern. Other materials used in the single cell are Gore 5621 MEA, reaction area 25 cm^2 (from Gore Tex Fuel Cell Co.) and brass current collector. The test cell configuration is shown in Fig. 1. The dimensions of components and operating conditions are consistent with the numerical model. The fuel cell test system is developed by Electrochem. Co.

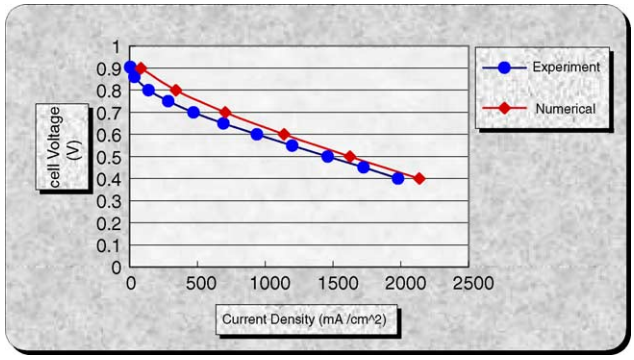

Fig. 3. Comparison of experiment with simulation polarization curves (serpentine flow pattern).

3. Results and discussions

The results of numerical simulation are validated with experimental data. The polarization curves of serpentine flow pattern at base operating condition are calculated, as shown in Fig. 3. The properties, parameters and base conditions of numerical simulation are listed in Tables 1 and 2, which are referred mainly from Bernardi and Verbrugge [2]. The relative deviation of current density of the modeling-predicted data with experimental data is less than 20% under high voltage 0.7 V, and 5% for low voltage 0.4 V. Since we neglect water flooding effect at the cathode side in the single-phase model, some data are slightly over predicted. However, the trend of increasing current density with decreasing the cell potential agrees well.

The polarization curves with various flow field patterns are shown in Fig. 4. The design of parallel straight pattern has less power density, around 2/3, comparing with serpentine and interdigitated flow patterns. In addition, the interdigitated flow pattern can enhance limiting current density due to the convective flow field at porous diffusion layer.

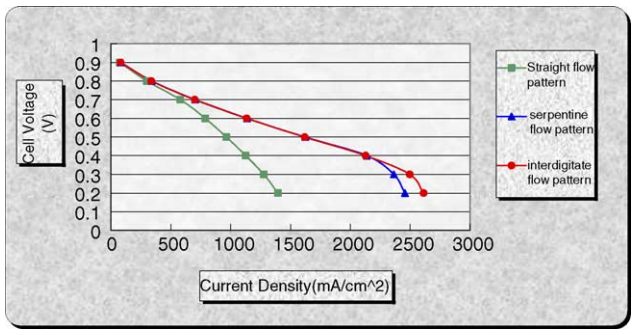

Fig. 4. Polarization curves of straight flow, serpentine flow and interdigitated flow patterns in the same operating conditions (numerical simulation).

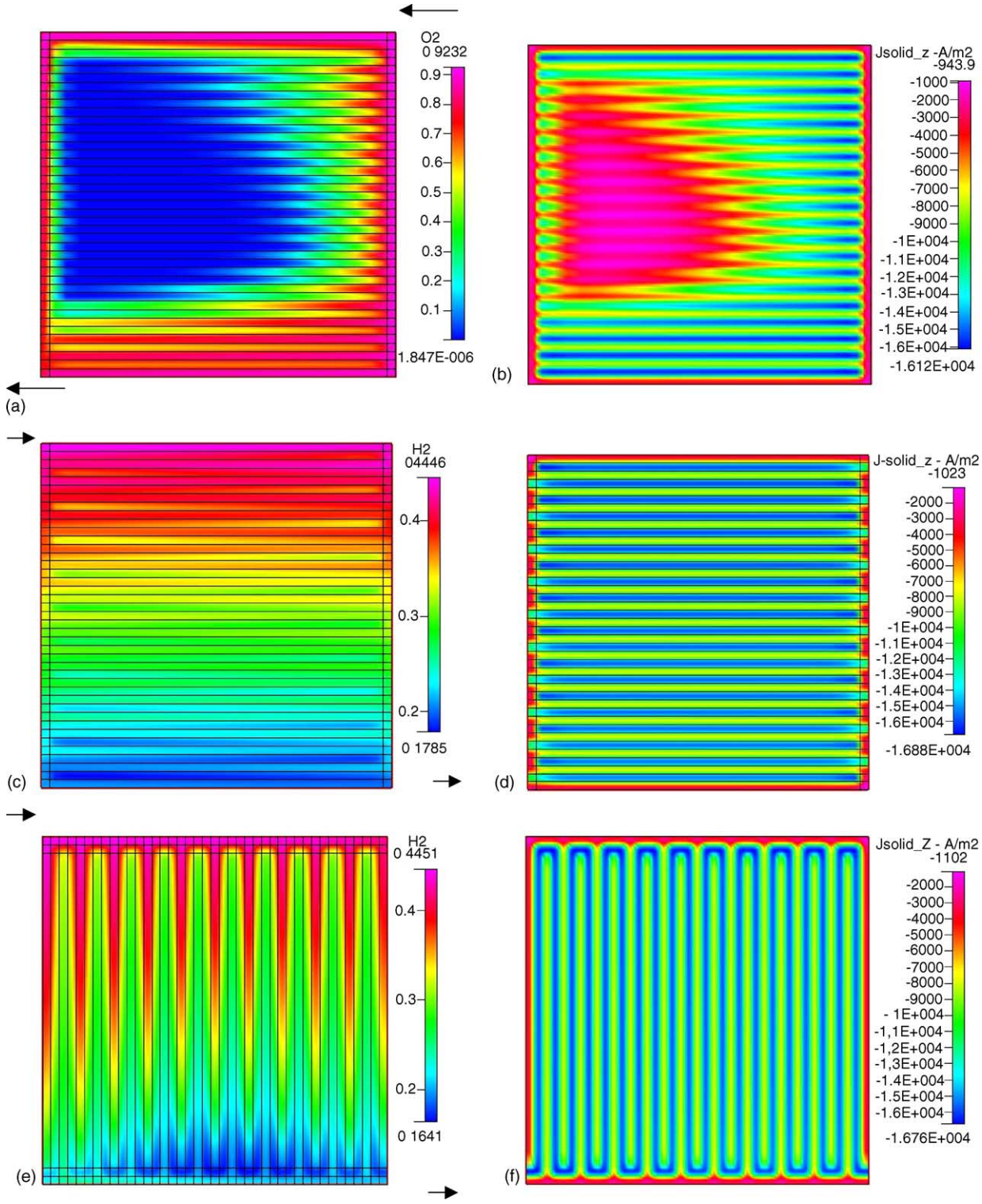

Fig. 5. Parallel straight flow (a) O_2 mass fraction, (b) current density, serpentine flow, (c) H_2 mass fraction, (d) current density and interdigitated flow, (e) H_2 mass fraction and (f) current density (0.6 V).

Fig. 5 displays the species concentrations and the current density distributions (operated at 0.6 V). Fig. 5(a) illustrates the non-uniform oxygen concentration distribution at cathode side for the parallel straight pattern. Lower oxygen concentration appears at cell center and left-top corner resulting low current density. Fig. 5(c and d) displays hydrogen concentration and current density of the serpentine flow pattern. The downstream of channel has lower hydrogen concentra-

tion, which also resulting low current density. Fig. 5(e and f) displays the hydrogen concentration and current density for interdigitated flow pattern. The hydrogen concentration and current density are higher and more uniform at inlet channel. On the contrary, the concentrations are significantly decreased at porous diffusion layer. The hydrogen concentration is depleted near outlet corner. The major pressure loss also appears at the cross-section of porous diffusion layer. It is noticed that the decrease of the rib width of flow channel will cause the decrease of the pressure and concentration drop. This leads to the uniformity of the concentration as well as the increase of cell performance. We suggest that the optimal value of the rib width over diffusion layer thickness around two. As the operating potential is smaller than 0.4 V, the non-uniform effect becomes more pronounced. Eventually, the membrane could dry out at high current density region.

Fig. 6 shows the numerical prediction of polarization curves at variable operating cell temperatures. The cell performance increases with temperature due to high membrane conductivity. This is contradicted with experimental results [10] with operating temperature above 70 °C. In the model, the membrane dry out situation is not considered at high cell temperature. However, higher fuel and oxygen temperatures could also induce more water vapor, resulting in lower hydrogen concentration at inlet. Therefore, the limiting current density decreases as fuel/oxygen temperatures increase.

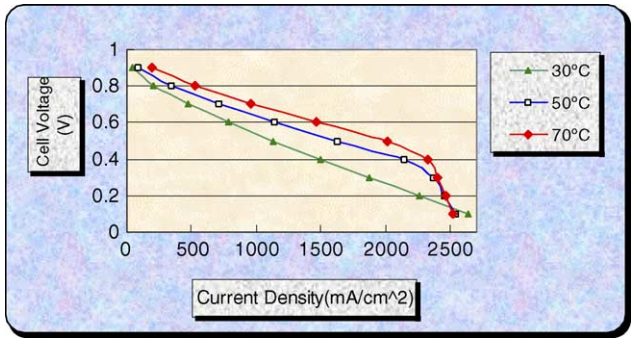

Fig. 6. Polarization curves of the fuel cell at variable operating temperatures (numerical simulation).

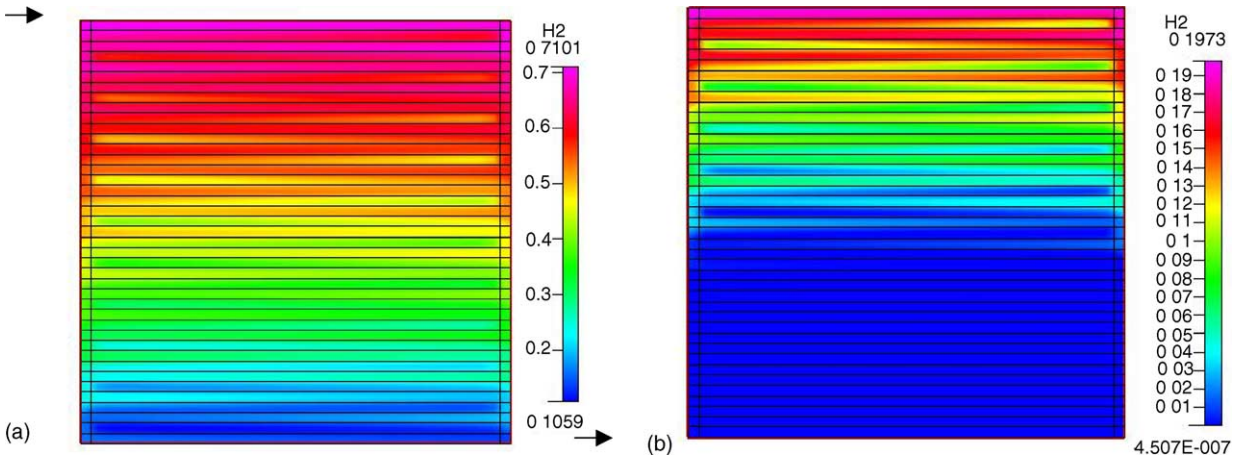

Fig. 7. H_2 mass fraction at operation voltage (0.2 V) and temperature: (a) 30 °C and (b) 70 °C.

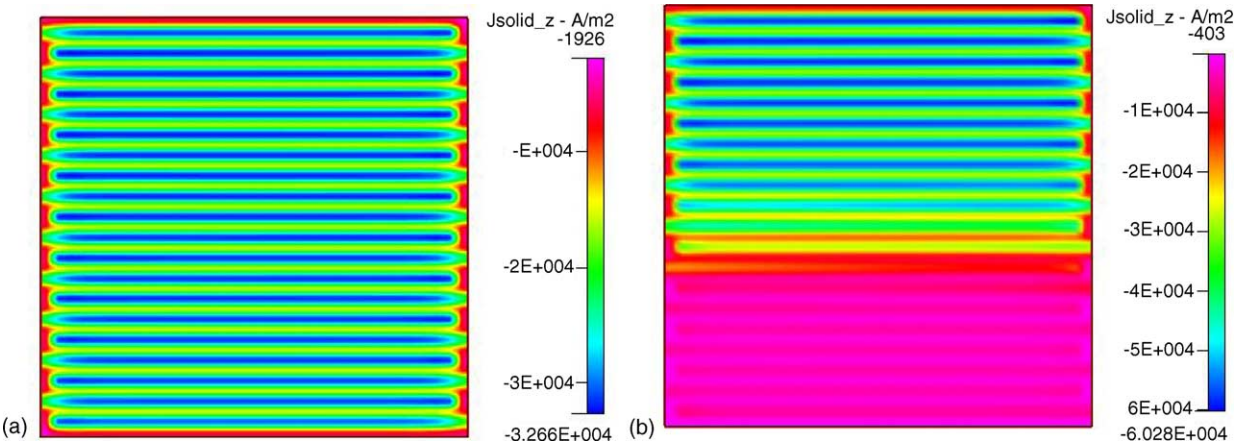

Fig. 8. Current density at operation voltage 0.2 V and temperature: (a) 30 °C and (b) 70 °C.

Figs. 7 and 8 display the hydrogen concentration and current density at 30 and 70 °C, respectively. The operating conditions are 0.2 V, 1 atm and flow rate is 300 $cm^3\,min^{-1}$. The high temperature of fuel cell has low ohmic resistance, and more active electrochemical reaction at upstream of flow channel. Therefore, the limiting current appears at downstream of flow channel. However, the concentration and current density become non-uniform. The membrane could dry out at high current density area due to the heat generation, which could lead an unstable cell performance.

Fig. 9 shows the polarization curves of the fuel cell at variable relative humidity. As the relative humidity is above 50%, the membrane conductivity is constant. The 100% relative humidity has higher limiting current than that of 50% humidity. The fuel cell needs high relative humidity as the fuel cell operating high current density. The membrane conductivity is a function of water content and temperature, which proposed by Springer et al. [1]. The numerical results show that membrane is dry out and high ohmic resistance without humidified fuel/oxygen gases.

Figs. 10 and 11 display the hydrogen concentration and current density distributions at low voltage (0.2 V) and variable relative humidity. Without humidified hydrogen/oxygen gases, the membrane has low conductivity and low current density. The current density at the downstream of flow channel increases due to the water generation by chemical reaction. On the other hand, with 100% relative humidity of hydrogen/oxygen gases, the hydrogen is fast consumed and depleted at downstream of flow channel. This leads to the decrease of current density. The operating condition of low

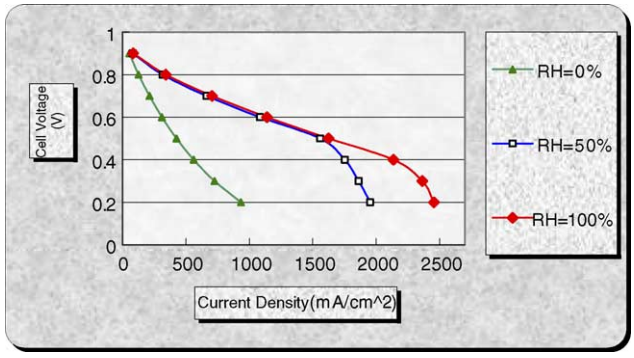

Fig. 9. Polarization curves of the fuel cell at variable relative humidity (numerical simulation).

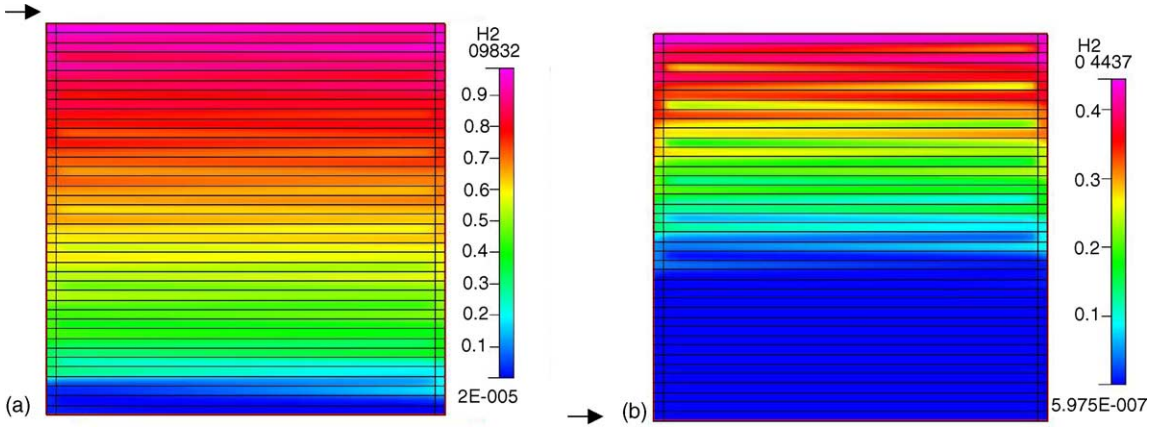

Fig. 10. H_2 mass fraction at operation voltage 0.2 V: (a) RH = 0% and (b) RH = 100%.

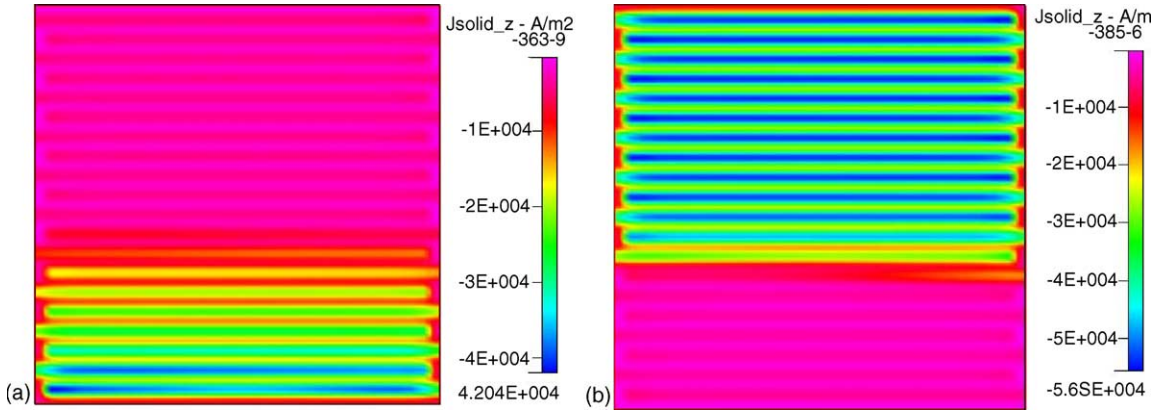

Fig. 11. Current density at operation voltage 0.2 V (a) RH = 0% and (b) RH = 100%.

humidity and high current density could lead an unstable cell performance.

4. Conclusions

A 3-D mathematical model to predict species concentration, current density distributions as well as cell performance is presented in this work. The model is based on the solution of the conservation equations of mass, momentum, species and electric current in a fully integrated finite-volume solver using the CFDRC commercial code. The influence of flow field pattern, cell temperature and humidity on the non-uniformity of species concentration, current is investigated. The polarization curve of serpentine flow pattern is well correlated with experimental data. The following conclusions are made:

1. The simulation results reveal that serpentine and interdigitated flow patterns show strong convection and high mass transfer. However, they also have higher pressure loss. In the interdigitated flow pattern, the cell performance, non-uniformity and pressure drop are strong dependent on the width of channel rib. Optimal design is important to improve its cell performance.
2. The cell performance increases with the temperature increase due to the high membrane conductivity. However, the membrane will dry out at high cell temperature.
3. Non-uniform distributions of gas concentration and current density appear at high temperature, high current density and low humidity operations, which could lead to an unstable cell performance.

Acknowledgments

We would like to acknowledge gratefully the financial support made by the Technology Development Program to Academia, the DIT, Taiwan, ROC, under Grant No. 91-EC-17-A-05-S1-0012.

References

[1] T.E. Springer, T.A. Zawod Inski, S. Gottesfeld, J. Electrochem. Soc. 138 (8) (1991) 2334–2342.
[2] D.M. Bernardi, M.W. Verbrugge, J. Electrochem. Soc. 139 (1992) 2477.
[3] V. Gurau, H. Liu, S. Kakac, AIChE J. 44 (1998) 2410–2422.
[4] D. Singh, D.M. Lu, N. Djilali, Int. J. Eng. Sci. 37 (1999) 431–452.
[5] T.V. Nguyen, R.E. White, J. Electrochem. Soc. 140 (8) (1993) 2178–2186.
[6] S. Um, C.Y. Wang, K.S. Chen, J. Electrochem. Soc. 147 (2000) 4485–4493.
[7] S. Mazumder, J.V. Cole, J. Electrochem. Soc. 150 (2003) A1503–A1509.
[8] A. Su, F.-B. Weng, Y.C. Chiu, Int. J. Energy Res. 29 (2005) 409–425.
[9] T. Beming, D.M. Lu, N. Djilali, J. Power Sources 106 (2002) 284–294.
[10] L. Wang, H. Liu, J. Power Sources 134 (2004) 185–196.
[11] G. Hu, J. Fan, S. Chen, Y. Liu, K. Cen, J. Power Sources 136 (2004) 1–9.
[12] M. Mench, C.Y. Wang, M. Ishikawa, J. Electrochem. Soc. 150 (2003) A1052–A1059.
[13] A. Hakenjos, H. Muenter, U. Wittsadt, C. Hebling, J. Power Sources 131 (2004) 213–216.
[14] R. Satija, D.L. Jacobson, M. Arif, S.A. Werner, J. Power Sources 129 (2004) 238–245.